Neuron, Vol. 32, 867–881, December 6, 2001, Copyright ©2001 by Cell Press

SLO-1 Potassium Channels Control Quantal Content of Neurotransmitter Release at the *C. elegans* Neuromuscular Junction

Zhao-Wen Wang,[2] Owais Saifee,[2] Michael L. Nonet, and Lawrence Salkoff[1]
Department of Anatomy and Neurobiology
Washington University School of Medicine
Campus Box 8108
660 S. Euclid Avenue
St. Louis, Missouri 63110

Summary

Six mutants of SLO-1, a large-conductance, Ca^{2+}-activated K^+ channel of *C. elegans*, were obtained in a genetic screen for regulators of neurotransmitter release. Mutants were isolated by their ability to suppress lethargy of an *unc-64* syntaxin mutant that restricts neurotransmitter release. We measured evoked postsynaptic currents at the neuromuscular junction in both wild-type and mutants and observed that the removal of SLO-1 greatly increased quantal content primarily by increasing duration of release. The selective isolation of *slo-1* as the only ion channel mutant derived from a whole genomic screen to detect regulators of neurotransmitter release suggests that SLO-1 plays an important, if not unique, role in regulating neurotransmitter release.

Introduction

Mechanisms controlling the release of neurotransmitters are of vital importance in the nervous system because such mechanisms may control synaptic strength and plasticity that are fundamental to higher brain function. Presynaptic nerve terminals contain a variety of K^+ channels, which are potential regulators of neurotransmitter release (reviewed by Meir et al., 1999), but it is unlikely that they are all equal in their tasks. An approach to determining which of these many channels regulate neurotransmitter release in vivo is to perform genetic studies using a model organism. The ease of obtaining mutants, in combination with the recent development of synaptic physiology techniques (Richmond et al., 1999; Richmond and Jorgensen, 1999), has made *C. elegans* an attractive model organism for studying roles of K^+ channels in neurotransmitter release. Indeed, *C. elegans* has proven to be an excellent system for studying the mechanisms involved in synaptic release. Several critical and highly conserved components of the synaptic release machinery were first discovered in *C. elegans*, including UNC-13 and UNC-18 (Gengyo-Ando et al., 1993; Kohn et al., 2000; Maruyama and Brenner, 1991; Richmond et al., 1999), and the vesicular acetylcholine transporter (Alfonso et al., 1993). In addition, many other critical components of the synaptic release machinery are conserved in *C. elegans* (Rand and Nonet, 1997), and important information regarding their molecular mechanisms of actions has been obtained by studying mutants in this species.

We devised a genetic screen to identify molecules which functionally modulate neurotransmitter release in vivo. Mutants were isolated based on their ability to relieve the block in neurotransmitter release of an *unc-64* syntaxin mutant by assaying for behavioral suppression of its paralyzed phenotype (Saifee et al., 1998). The screen successfully identified targets previously implicated in regulating release, including a calcium- and calmodulin-dependent protein kinase II, a q-type α subunit of a G protein, and an adenylyl cyclase (O.S. and M.L.N., unpublished data; Chapman et al., 1995; Lackner et al., 1999; Zhong and Wu, 1991). These results demonstrate a proof of principle that the screen would successfully isolate regulators of neurotransmitter release. However, in addition to identifying these regulators, a single ion channel (the *C. elegans* SLO-1 BK channel) was also functionally identified as a regulator of release. Although more than 70 genes encoding K^+ channels exist in *C. elegans* (Salkoff, et al., 1999; Wei et al., 1996), only mutants in the SLO-1 K^+ channel were isolated in this screen, suggesting that *slo-1* BK channels may differ from other K^+ channels in their ability to regulate transmitter release.

Among K^+ channels, SLO-1 is an excellent candidate to play an important role in controlling neurotransmitter release because it is activated by Ca^{2+} as well as membrane depolarization. These channels are prominent at presynaptic nerve endings in many types of neurons (Anderson et al., 1988; Farley and Rudy, 1988; Katz et al., 1995; Knaus et al., 1996; Lindgren and Moore, 1989; Morita and Barrett, 1990; Robitaille et al., 1993; Sivaramakrishnan et al., 1991; Sun et al., 1999; Tabti et al., 1989; Vatanpour and Harvey, 1995; Wangemann and Takeuchi, 1993; Yazejian et al., 1997; Zhou et al., 1999) and have been found to colocalize with voltage-gated calcium channels at sites of transmitter release (Issa and Hudspeth, 1994; Robitaille et al., 1993). As Ca^{2+} entry through these channels may contribute to the activation of BK channels, the functional coupling of these two channels may exist, which could serve to regulate neurotransmitter release. Blockade of BK channels using charybdotoxin or iberiotoxin has been shown to increase the amplitude of evoked end-plate potentials at neuromuscular junctions in mouse and frog (Anderson et al., 1988; Marshall et al., 1994; Robitaille et al., 1993), although differing results have also been obtained (Fischer and Saria, 1999; Pattillo et al., 2001; Warbington et al., 1996).

In the present study, we describe our characterization of mutants in the *C. elegans* SLO-1 BK channel that relieve the synaptic transmission defects of a hypomorphic syntaxin mutant. These mutants result in the genetic removal of the SLO-1 BK channels, allowing study of the functional role of this channel. A combination of genetic, pharmacological, and electrophysiological analyses revealed that *slo-1* mutants were associated with increased quantal content of neurotransmitter release, which partially compensated for the reduced re-

[1] Correspondence: salkoffl@thalamus.wustl.edu
[2] These authors contributed equally to this work.

lease of the *unc-64* mutation. Because it was the sole K^+ channel identified in this screen, SLO-1 is likely to have major, if not unique, importance among K^+ channels as a regulator of neurotransmitter release in *C. elegans* and possibly in other systems.

Results

To identify proteins capable of modulating synaptic transmission, we performed a genetic screen for mutants that enhanced synaptic transmission in an *unc-64* syntaxin mutant background. While complete lack of *unc-64* syntaxin results in lethality, hypomorphic lesions result in viable animals that are lethargic and resistant to inhibitors of acetylcholinesterase. These defects are most likely due to a reduction in neurotransmitter release. We screened for suppression of *unc-64(e246)* syntaxin mutant paralysis and isolated six noncomplementing alleles that we mapped to the *C. elegans* ortholog of the large-conductance, Ca^{2+}- and voltage-dependent K^+ channel. We named this locus *slo-1*. Two additional alleles (*md1715* and *md1745*), which were isolated in a screen for suppressors of *ric-8* and mapped to a similar region of the genome (K. Miller, personal communication), were kindly provided by Kenneth Miller and James Rand.

SLO-1 Is a Large-Conductance, Ca^{2+}-Activated K^+ Channel

The primary sequence of SLO-1 shows a high level of identity to BK channels of the mouse (58.4%) (Butler et al., 1993), the human (58.6%) (McCobb et al., 1995; Pallanck and Ganetzky, 1994; Tseng-Crank et al., 1994), and *Drosophila* (66.1%) (Adelman et al., 1992). All of the major structural motifs of BK channels are present, including the seven membrane-spanning domains (S0–S6), a pore domain that contains the K^+ selectivity filter, a "Ca^{2+} bowl" that is important for sensing Ca^{2+} (Schreiber and Salkoff, 1997), and four hydrophobic segments in the C-terminal region (Figures 1A and 1B).

SLO-1 has at least three splice variants. In addition to the SLO-1a cDNA (Wei et al., 1996), two other splice variants were identified. Exon/intron boundaries of *slo-1* transcripts were determined by comparing cDNA sequences with genomic DNA sequence. SLO-1a (GenBank AF431891) is encoded by 20 exons and has a predicted length of 1140 residues. Compared with SLO-1a, SLO-1b (GenBank AF431892) lacks exon 13 and is 22 residues shorter. SLO-1c (GenBank AF431893) also lacks exon 13. In addition, it has an alternative exon 9 and an additional small exon following exon 11. The sequence and sites of alternative exons are showed in Figure 1A.

Biophysical properties of SLO-1a and SLO-1b were examined by heterologous expression in *Xenopus* oocytes. Both single channel and macroscopic currents were recorded from inside-out patches (Figure 2). As with BK channels from other species, channel activity increased with either elevation of [Ca^{2+}] on the cytoplasmic side of the patch (Figure 2B, left) or increase of membrane depolarization (Figure 2B, right). Elevating [Ca^{2+}] shifted the voltage range of activation to a more negative range (Figure 2A, right). Single channel conductance was estimated to be ~250 pS based on measurements of single channel current amplitudes in symmetrical K^+ solutions. However, precise determination of conductance was difficult due to the very brief mean open time of the channel, which is estimated to be less than 0.5 ms. No apparent differences in functional properties were observed between SLO-1a and SLO-1b (functional properties of SLO-1c were not examined). These observations showed that SLO-1 is similar to BK channels from other species, with regard to functional properties as well as amino acid sequence.

slo-1 Alleles Isolated as *unc-64* Suppressors Are Loss-of-Function Mutations

All of the *slo-1* mutants isolated in our genetic screen are recessive suppressors of *unc-64* paralysis. The *slo-1(md1745)* allele isolated from the *ric-8* suppressor screen also acted as a recessive suppressor of *unc-64* paralysis. All alleles had a similar behavioral phenotype, which could be rescued by germline transformation with wild-type *slo-1* (see below). Using primers designed according to SLO-1 cDNA sequences, we amplified first-strand cDNAs by RT-PCR and sequenced the products to identify molecular lesions in the mutants. Most lesions resulted in premature termination of the channel. Both *slo-1(md1745)* and *slo-1(js379)* contained nonsense lesions early within the gene prior to the ion-conducting channel pore. This would preclude formation of functional channels and therefore likely result in the *slo-1* null phenotype. In *slo-1(js118, js380, js381)*, the channel was truncated prior to the highly conserved carboxy-terminal "Ca^{2+} bowl" region. In contrast, *slo-1(md1715)* contained a single nucleotide mutation resulting in a glycine-to-glutamate change on the extracellular face of the channel (Figure 1B).

Although the molecular lesions of *slo-1(md1745)* and *slo-1(js379)* were clearly expected to eliminate channel function, the functional consequences of other mutations were less clear and therefore subjected to further analysis. The mutations found in *slo-1(md1715)* and *slo-1(js118)* were introduced independently into the SLO-1a cDNA, and the resulting mutant channels were subjected to physiological analysis in the *Xenopus* oocyte system. No BK channel activity was detected in either mutant channel in contrast to wild-type controls. This suggests that these mutations also resulted in a complete loss of function (data not shown). The mutant alleles *slo-1(js380, js381)* truncated the channel at a similar location as *slo-1(js118)* and, hence, were also expected to remove channel function. We conclude then that all mutants isolated by virtue of their ability to suppress the *unc-64* phenotype most likely conferred the same physiological phenotype, the complete removal of the SLO-1 current from the membrane.

slo-1 Mutations Suppress the Behavioral Deficits of Syntaxin Mutant

slo-1 mutants suppress the lethargy of *unc-64* mutants. Measurements of locomotion velocity of *unc-64* single mutants showed greatly decreased velocity and indifference to mechanical stimulation (Figure 3A). Addition of *slo-1* mutations resulted in a modest increase of general activity, but a dramatic improvement in stimulation pro-

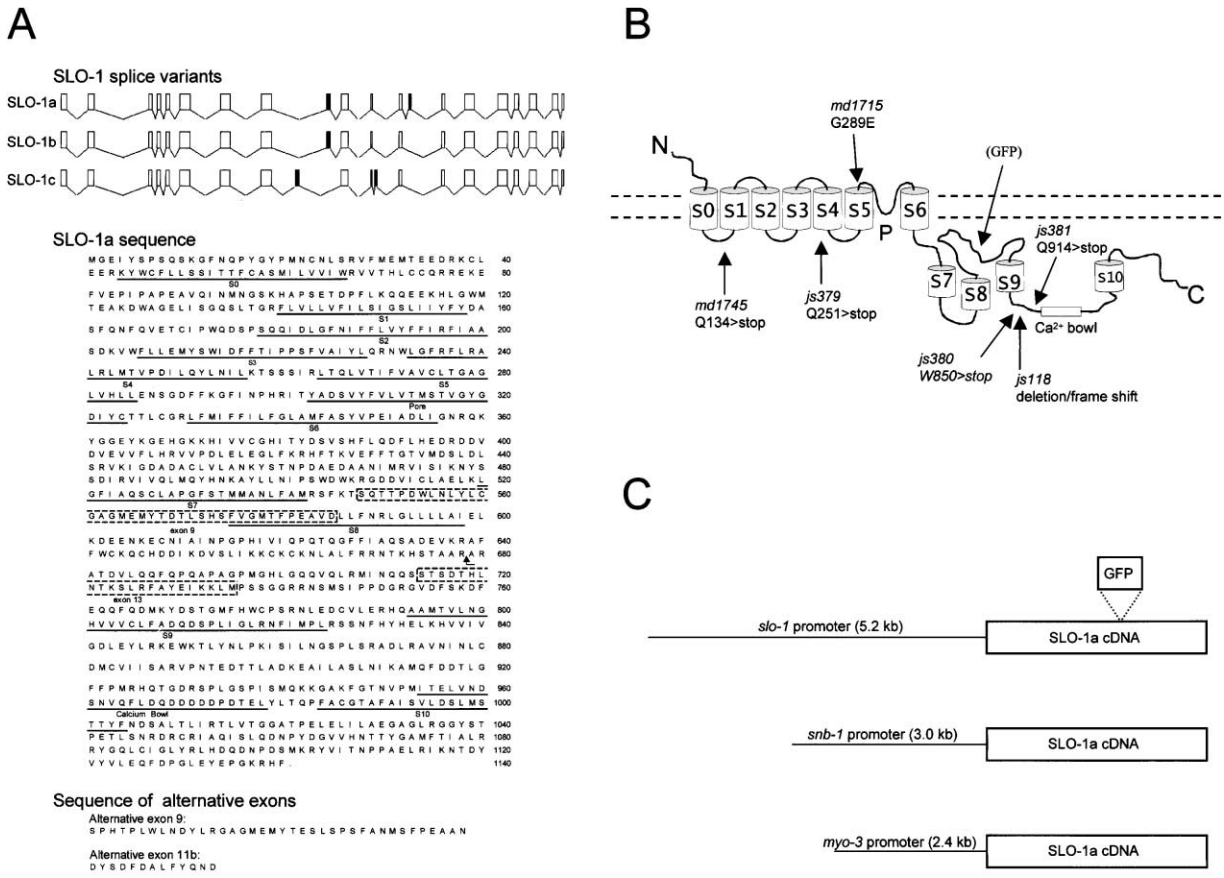

Figure 1. The Primary Sequence of SLO-1, Mutant Alterations, and Splice Variants

(A) The primary sequence of SLO-1. (Top) SLO-1 splice variants shown schematically. The boxes represent exons, and lines represent introns. The open boxes represent exons common to all splice variants, whereas the filled boxes represent alternative exons. Compared with SLO-1a, SLO-1b lacks exon 13. SLO-1c, besides the lack of exon 13, uses an alternative exon 9, as well as an additional exon (exon 11b) following exon 11. (Middle) The complete sequence of SLO-1a is shown. Major structural domains characteristic of BK channels, including 11 hydrophobic segments (S0–S10), the pore, and the Ca^{2+} bowl, are underlined. Two alternative exons (exons 9 and 13) are outlined with broken lines. The position of the insertion of exon 11b is marked by an arrow in the SLO-1a sequence. (Bottom) Sequences of alternative exons.

(B) Predicted membrane topology of SLO-1. Major structural domains and locations of identified mutations are indicated. All mutations, except for *md1715*, resulted in premature termination of the protein due to either nonsense mutations (*js379, js380, js381, md1745*) or deletion plus frame shift (*js118*). A glycine to glutamate missense mutation occurred in *md1715.* In *js118*, exon 16 was absent due to a 271 bp deletion in genomic DNA that removes most of exon 16 and a portion of the previous intron. The location of GFP insertion in the *slo-1* minigene (see Figure 1C) is also indicated.

(C) Schematic depiction of minigenes used in germline transformation. SLO-1a cDNA was ligated to promoters from three different genes: *slo-1*, *snb-1* (neuron specific), and *myo-3* (body-wall muscle specific). GFP was inserted between S8 and S9 of SLO-1 (by replacing L706 and R707 with GFP) in experiments examining SLO-1 in vivo expression patterns.

voked locomotion. *slo-1* suppression of locomotion defects of *unc-64(e246)* was not allele specific, as *slo-1* mutations also enhanced movement of *unc-64(js21)* (Saifee et al., 1998) animals (data not shown). This increased movement was not due to simple hyperactivity resulting from the *slo-1* mutant, as *slo-1* single mutants did not move faster than wild-type animals. On the contrary, *slo-1* single mutants appeared similarly active as wild-type animals, but their movement was less smooth and was characterized by an increased tendency to stop and reverse direction. Such reversals of direction reduced the apparent net distance traveled between successive captured images (see Experimental Procedures), thereby resulting in a slight reduction in average velocity (Figure 3B). Although *slo-1* mutants themselves had only subtle behavioral phenotypes, they mitigated the behavioral deficits of syntaxin mutants. This suppression most likely resulted from compensation of the transmission defect in the syntaxin mutant.

Pharmacological assessment of acetylcholine release supports the hypothesis that loss of SLO-1 increases neuromuscular transmission in the syntaxin hypomorph. The acetylcholinesterase inhibitor aldicarb potentiates the effect of released acetylcholine by blocking its degradation (Rand and Russell, 1985). In wild-type animals, the accumulation of acetylcholine results in tonic contraction of body-wall muscle, which, over time, leads to a hypercontracted paralysis. Mutants with reduced acetylcholine release, such as *unc-64*, are resistant to the hypercontraction induced by aldicarb (Miller et al., 1996; Saifee et al., 1998). In combination with various *slo-1* alleles, the sensitivity of *unc-64* to aldicarb was

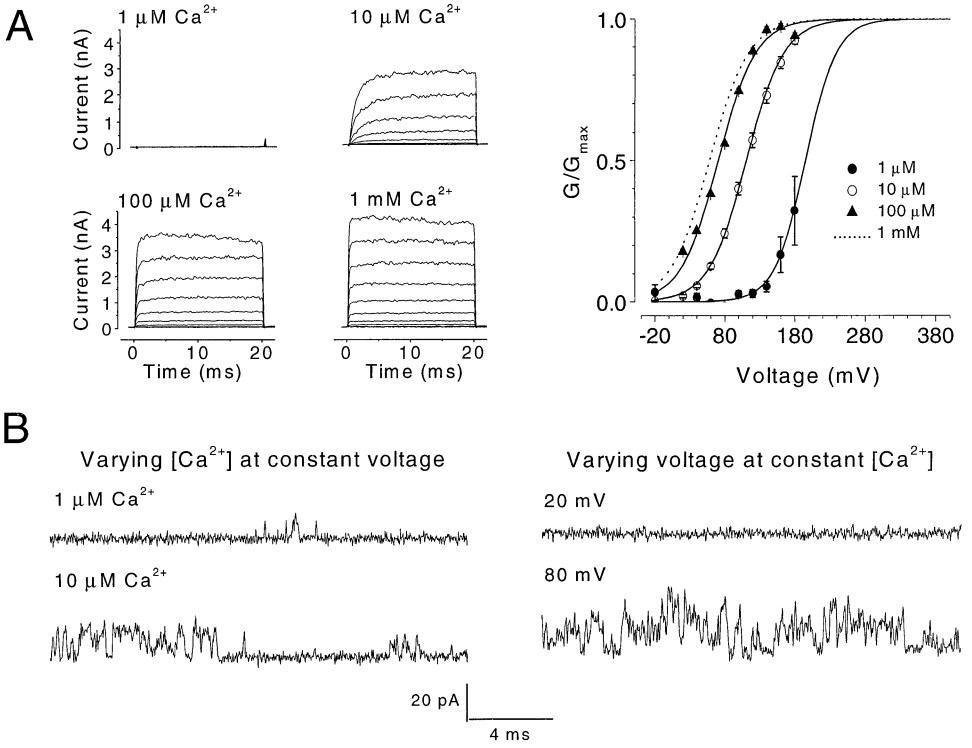

Figure 2. SLO-1 Heterologously Expressed in *Xenopus* Oocytes Is Activated by Cytoplasmic Ca^{2+} and Membrane Depolarization

(A) (Left) Macroscopic currents of an inside-out patch in response to changes of membrane potential and cytoplasmic [Ca^{2+}]. The membrane was held at −60 mV and step pulses were applied from −40 to +180 mV in 20 mV steps. Traces shown are from voltage steps of −40 to +140 mV. (Right) Conductance-voltage relationships of macroscopic currents at different $[Ca^{2+}]_o$. Data was fitted to a Boltzmann function. The fit at 1 mM $[Ca^{2+}]_o$ was extrapolated from only four data points to avoid deviation from the true conductance-voltage relationship due to the blocking effect of Ca^{2+} at higher holding potentials. The voltage for half-maximal activation (V_{50}) was 58 ± 5 mV at 1 mM [Ca^{2+}] (n = 12), 71 ± 3 mV at 100 μM [Ca^{2+}] (n = 16), 111 ± 1 mV at 10 μM [Ca^{2+}] (n = 16), and 201 ± 2 mV at 1 μM [Ca^{2+}] (n = 8).

(B) Representative traces of single channel currents from inside-out patches. (Left) Changing [Ca^{2+}] while holding the membrane potential constant (+80 mV). (Right) Changing membrane potential while keeping [Ca^{2+}] constant (100 μM). Results shown are of the SLO-1a splice variant.

shifted toward that of wild-type (Figure 3C). Thus, in addition to suppressing lethargy, *slo-1* mutants also suppressed the *unc-64* resistance to aldicarb, which further indicates an enhancement of neuromuscular transmission in the double mutant. By contrast, *slo-1* single mutants more rapidly succumbed to aldicarb treatment than wild-type animals (Figure 3D), showing an increased sensitivity to aldicarb. Hypersensitivity to aldicarb is suggestive of increased neurotransmitter release in *slo-1* mutants, which can explain their ability to act as suppressors of syntaxin mutants. This observation is consistent with SLO-1 normally acting to limit the amount of transmitter release.

slo-1 mutations also suppressed synaptic transmission defects in the pharynx of *unc-64* mutants, as revealed by recordings of electropharyngeograms (EPGs). EPGs are extracellular recordings from the pharynx that allow study of synaptic transmission between the M3 motor neuron, a glutamatergic inhibitory neuron regulating the duration of pharyngeal muscle contraction, and the pharyngeal muscle (Avery, 1993; Dent et al., 1997; Raizen and Avery, 1994). A typical EPG from the wild-type contains three to five M3 inhibitory postsynaptic potentials (IPSPs) (Figure 3E). The M3 IPSPs of *unc-64(e246)* were reduced in amplitude (Figure 3E and Saifee et al., 1998). Introduction of a *slo-1* mutant into this syntaxin mutant background increased IPSP amplitudes (Figure 3E), resulting in EPGs that were reminiscent of wild-type. *slo-1* mutations therefore compensated for the reduced efficacy of release of the syntaxin mutant in the pharynx. EPGs from *slo-1* single mutants appeared grossly wild-type, with the only difference among them being a slightly shorter duration (Figure 3E). This shorter duration could reflect enhanced M3 motor neuron neurotransmission that hastened repolarization of the pharyngeal muscle. Thus, SLO-1 acts to modulate neuromuscular transmission in the pharyngeal as well as body-wall muscle.

SLO-1 Functions Presynaptically to Modulate Neurotransmission

In order to understand the mechanism of SLO-1 action in synaptic transmission, we began by investigating its cellular localization. The tissue distribution of SLO-1 was assessed using a polyclonal antiserum raised against a portion of the Ca^{2+} bowl of the mouse BK channel (mSlo) (Knaus et al., 1995). As this 14-residue region of SLO-1 (residues 953–966) differs from mSlo by only a single residue, the antiserum was expected to crossreact with the *C. elegans* ortholog. Staining of wild-type animals

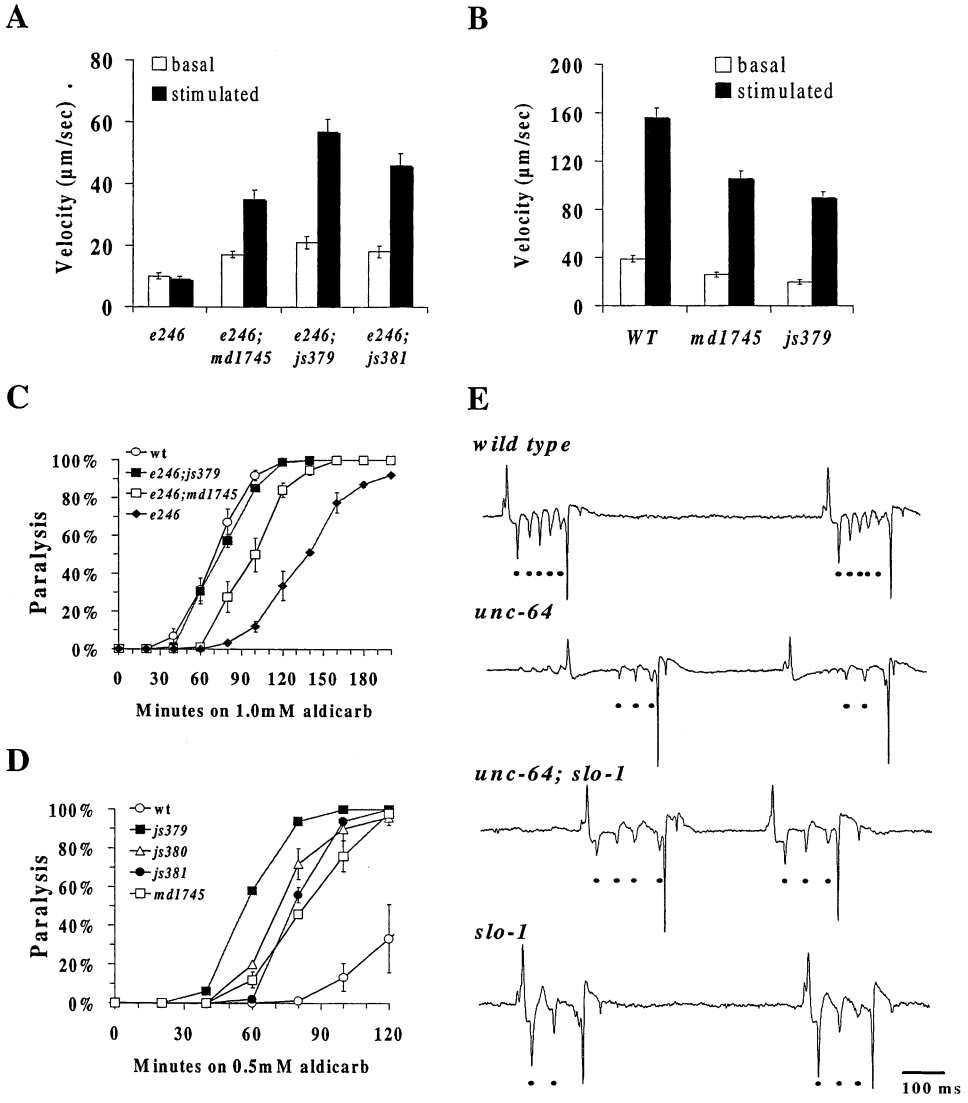

Figure 3. *slo-1* Mutants Suppress Behavioral, Pharmacological, and Pharyngeal Electropharyngeogram (EPG) Defects of the Syntaxin Hypomorph *unc-64(e246)*

(A) Measurements of locomotion velocities for *unc-64* mutant and *unc-64;slo-1* double mutants. Unstimulated (white bars) and stimulated (black bars) velocities (mean ± SE) were calculated from measurements of 20–25 animals.

(B) Measurements of locomotion velocities for wild-type and *slo-1* mutants. Velocities (mean ± SE) were calculated from measurements of 20–25 animals.

(C) Aldicarb sensitivity of *unc-64* mutant and *unc-64;slo-1* double mutants. The time course of paralysis is shown for wild-type, *unc-64*, and selected *unc-64;slo-1* double mutants on 1.0 mM aldicarb plates seeded with *E. coli*. Values represent mean ± SE.

(D) Aldicarb sensitivity of wild-type and *slo-1* mutants. The time course of paralysis is shown for wild-type and selected *slo-1* mutants on 0.5 mM aldicarb plates seeded with *E. coli*.

(E) Physiological recordings of pharyngeal muscle activity. Characteristic electropharyngeograms are shown from wild-type, *unc-64, unc-64;slo-1(js100),* and *slo-1(js100)*. Filled circles indicate M3 motor neuron-induced IPSPs. All traces are millivolts versus time.

revealed immunoreactivity in synaptic regions of the nervous system including in both the nerve ring (Figure 4A) and nerve cords, as well as in the body-wall (Figure 4C) and vulval muscle. The staining in the body-wall muscle was restricted and appeared as puncta, which is reminiscent of the localization pattern of ryanodine receptors (Maryon et al., 1998). In *C. elegans*, ryanodine receptors are localized to surface membrane associated sacs located between M line analogs and dense bodies (Z line analogs). These membrane sacs resemble junctional sarcoplasmic reticulum of vertebrate skeletal and cardiac muscle (Waterston, 1988; Maryon et al., 1998). We do not have direct evidence suggesting a relationship between SLO-1 and the other structures. *slo-1* mutants were found to lack immunoreactivity (data not shown), indicating the specificity of the antibody. A similar pattern of SLO-1 expression (Figures 4B and 4D) was observed in animals transformed with a *slo-1* fusion to GFP (Figure 1C). The presence of SLO-1 in the nerve ring where the density of synapses is high, and its pres-

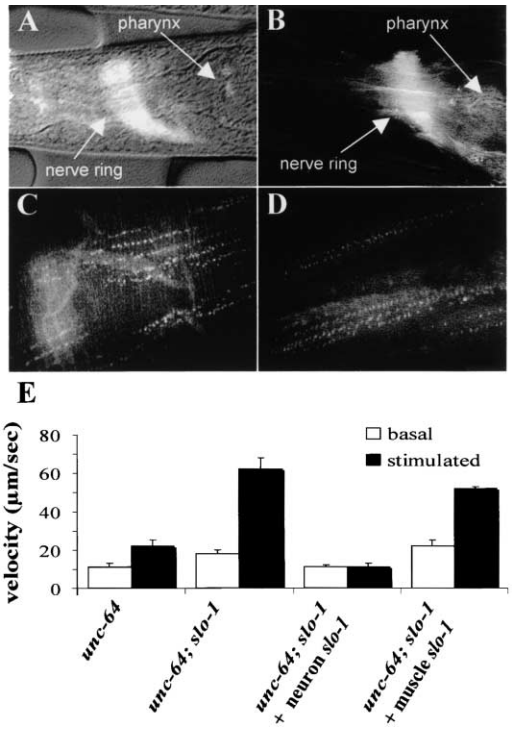

Figure 4. *slo-1* Expression in Neurons and Muscle, and Neuron-Specific Effects on Locomotion

(A–D) *slo-1* expression and protein localization. (A and C) Whole adult wild-type hermaphrodite worms fixed and stained with anti-BK channel primary antibodies and visualized with FITC-conjugated secondary antibodies. Lateral view showing dense staining in the synapse-rich nerve ring in the head region (A) and punctate immunoreactivity near the surface of body-wall muscle (C). (B and D) Fluorescence images from live wild-type adult hermaphrodite animals expressing the SLO-1*a::GFP* fusion as an extrachromosomal array. Lateral view showing bright fluorescence in the nerve ring (B) and punctate fluorescence near the surface of body-wall muscle (D).

(E) Impact of tissue-specific rescue of *slo-1* on locomotion. Locomotion velocities of *unc-64*, *unc-64;slo-1(js118)*, and two transgenic strains of *unc-64;slo-1(js118)* transformed with a SLO-1a minigene under the control of either the *snb-1* promoter driving expression selectively in neurons or the *myo-3* promoter driving expression selectively in body-wall muscle.

ence in motor neurons is consistent with a role in controlling synaptic release at both interneuronal synapses and neuromuscular junctions (NMJs).

Because *slo-1* is expressed in both neurons and body-wall muscle, suppression of syntaxin paralysis could result from either loss of SLO-1 in neurons, or muscle, or both. In order to determine where SLO-1 was modulating synaptic transmission, we used tissue-specific promoters to selectively drive expression of a rescuing SLO-1 construct in all neurons (including motor neurons) or in body-wall muscle. When functional SLO-1 was reintroduced into neurons, suppression was removed and the paralyzed phenotype of the syntaxin mutant returned (Figure 4E). On the other hand, there was no detectable effect on locomotion when SLO-1 was expressed in body-wall muscle, i.e., those animals remained suppressed (Figure 4E). The neuron-specific rescuing construct had no appreciable effect in wild-type animals (data not shown). Thus, at the NMJ, SLO-1 likely acts presynaptically in motor neurons to limit neurotransmitter release.

slo-1 Mutations Increase Neurotransmitter Release

As described, *slo-1* mutants exhibited increased sensitivity to aldicarb (Figure 3), a phenotype most likely due to enhanced acetylcholine release. To determine whether neurotransmitter release was indeed increased at the NMJ in *slo-1* mutants, we compared synaptic output between wild-type and *slo-1* mutant animals. Evoked excitatory postsynaptic currents (EPSC) were recorded from voltage-clamped body-wall muscle cells. EPSCs were evoked by stimulating the presynaptic motorneuron with 0.5 ms DC pulses provided through a glass micropipette (5–7 MΩ) (see Experimental Procedures). Spontaneous miniature excitatory postsynaptic currents (mEPSC) were also recorded. To quantify the change in neurotransmitter release, we measured amplitude, duration, and quantal content of EPSCs. Quantal content was estimated by dividing the current integral (current over time) of an EPSC by the average current integral of mEPSCs.

Analysis of EPSCs from wild-type animals in an extracellular solution containing high Ca^{2+} (5 mM) showed a large and synchronous postsynaptic current averaging 1155 ± 183 pA. In the *slo-1* mutant, the response was also large (806 ± 107 pA), and not statistically different (Figures $5A_a$ and $5A_c$). The kinetic properties of EPSCs were grossly similar between the wild-type and the *slo-1* mutant. However, the duration of EPSCs appeared longer in the *slo-1* mutant due to the presence of a persistent component (insets, Figure $5A_a$). This persisting component was difficult to quantify due to its small amplitude (in comparison with the EPSC peak amplitude) and irregularity in shape. Nevertheless, it suggested to us that neurotransmitter release might be prolonged in *slo-1* mutants.

We reasoned that a difference in neurotransmitter release between *slo-1* mutants and the wild-type might be more obvious under experimental conditions where EPSC quantal content was lower. This is because under high Ca^{2+} conditions, the evoked response may entail the release of nearly the entire population of readily releasable vesicles. Therefore, no additional synaptic vesicles could be released even if the removal of SLO-1 would augment Ca^{2+} entry into the presynaptic terminal. To test this hypothesis, we examined EPSCs induced by repetitive 7 Hz stimulation in wild-type preparations at high $[Ca^{2+}]_o$ (5 mM). As shown in Figure $5B_a$, the EPSC amplitude was large in the first stimulation, but decreased drastically thereafter. In contrast, EPSC amplitude remained constant in wild-type preparations in response to 10 Hz repetitive stimulation at 250 μM $[Ca^{2+}]_o$ (Figure $5B_a$). Similarly, constant EPSCs were observed in the *unc-64* mutant at 5 mM $[Ca^{2+}]_o$ in response to repetitive stimulation (data not shown). Thus, consistent with our hypothesis, these observations suggest that the readily releasable pool of synaptic vesicles was nearly depleted in response to a single stimulus at high $[Ca^{2+}]_o$ (but not at low $[Ca^{2+}]_o$) in wild-type animals and that depletion did not occur at high $[Ca^{2+}]_o$ in the *unc-64* mutant. This hypothesis was also supported by experi-

ments with 4-aminopyridine (4-AP) at 5 mM $[Ca^{2+}]_o$ (Figure 5B$_b$). 4-AP blocks several K^+ channels including the Shaker type (Mathie et al., 1998), which has been implicated in the control of neurotransmitter release (Jan et al., 1977). To characterize the effect of 4-AP, we measured both the amplitude and the decay time constant of the EPSCs prior to and following the application of 4-AP. A time constant (τ) was obtained by fitting the first 20 ms decaying phase of EPSCs with a single exponential. A larger τ value would indicate an increased EPSC duration. The decay time constant did not differ between the wild-type and the *slo-1* mutant in the absence of 4-AP. In wild-type animals, neither the amplitude nor the τ value of EPSCs was altered by 4-AP. In the *slo-1* mutant, however, we noted a decrease in amplitude but a significantly increased τ value following 4-AP application. However, the quantal content of the *slo-1* mutant changed little since the increase in decay time constant was offset by a decrease in EPSC amplitude, suggesting that EPSC quantal content was essentially maximized at 5 mM $[Ca^{2+}]_o$. The prolongation of decay time constant by 4-AP in *slo-1* mutant (but not wild-type animals) suggests that both SLO-1 and 4-AP-sensitive K^+ channels likely regulate neurotransmitter release at the NMJ. However, their functions may be somewhat redundant such that blockade of one channel type had little effect on the release, but inhibition of both types had a large effect. The amplitude and quantal content of EPSCs were also not increased by tetraethylammonium in wild-type animals (data not shown), consistent with our hypothesis that the readily releasable pool of vesicles was nearly depleted in response to a single impulse in 5 mM $[Ca^{2+}]_o$.

As the above results implied a rapid depletion of vesicles at high $[Ca^{2+}]_o$, we undertook experiments to examine the effect of *slo-1* mutations under conditions where we could be confident that the readily releasable pool would not be depleted. Thus, we examined the effect of *slo-1* mutations on EPSCs at a reduced external Ca^{2+} concentration (250 μM $[Ca^{2+}]_o$ and 4 mM $[Mg^{2+}]_o$) (Figure 6). Under these conditions, the evoked wild-type EPSC appeared as a cluster of overlapping mEPSCs. In wild-type animals, EPSCs averaged 33.6 $\pm$ 7.4 pA in amplitude and 46.9 $\pm$ 4.6 ms in duration. In marked contrast, the *slo-1* mutant showed a significant increase in the duration (86.9 $\pm$ 15.4 ms) of EPSC. The EPSC amplitude (64.4 $\pm$ 17.7 pA) was also increased with marginal statistical significance ($p = 0.121$). As a result, the estimated quantal content of the mutant EPSC (36.1 $\pm$ 8.1) was 4-fold greater than that of the wild-type (8.5 $\pm$ 1.1). These observations clearly indicated that neurotransmitter release was increased at the NMJ in the *slo-1* mutant.

In contrast to this large difference in evoked release, the mEPSC frequency was similar between the wild-type and *slo-1* mutant at either concentration of external Ca^{2+}. At high (5 mM) $[Ca^{2+}]_o$, the frequencies were 48.0 $\pm$ 8.1 s^{-1} and 47.8 $\pm$ 4.2 s^{-1} in wild-type and *slo-1*, respectively (Figures 5A$_b$ and 5A$_c$). At reduced (250 μM) $[Ca^{2+}]_o$, the frequency was 24.0 $\pm$ 6.4 s^{-1} in the wild-type and 32.9 $\pm$ 7.4 s^{-1} in the mutant (Figures 6B and 6C). The average amplitude and area of mEPSCs of *slo-1* mutants were similar to those of wild-type (details in the legends of Figures 5 and 6). Because mEPSCs were unchanged, the enhancement of synaptic transmission, as evidenced by the increased evoked response, was most likely due to an increase in neurotransmitter release rather than a change in muscle sensitivity.

Reduced Neurotransmitter Release in *unc-64* Mutants, and Partial Rescue by *slo-1*

We characterized the release defects of the single *unc-64* and double *unc-64;slo-1* mutants at the NMJ to further investigate the physiological basis of the suppression of the syntaxin mutant by *slo-1* lesions. Syntaxin is a core component of the vesicle fusion machinery. Consistent with such a role, we found that both the frequency of mEPSCs and the amplitude of EPSCs were much lower in the *unc-64* mutant than in the wild-type under similar experimental conditions (5 mM $[Ca^{2+}]_o$) (compare Figure 7 with Figure 5A). The frequency of mEPSCs was 10 $\pm$ 2 s^{-1} in the *unc-64* mutant, $\sim$20% of the wild-type value. The amplitude of *unc-64* EPSCs averaged 143.2 $\pm$ 33.8 pA, which was only 12% of the wild-type EPSC amplitude. Estimated quantal content in *unc-64* (10.6 $\pm$ 1.4) was only 5% of wild-type. Because quantal content was so radically reduced, the evoked response appeared as an asynchronous cluster of mEPSCs. The greatly reduced quantal content of EPSCs at the *unc-64* NMJ is consistent with the strong locomotion defect of these animals.

Removal of SLO-1 increased neurotransmitter release by approximately 4-fold in the *unc-64* mutant (Figure 7). Quantal content of EPSCs was 43.5 $\pm$ 11.6 in *unc-64; slo-1* double mutants. This increase in quantal content was due to an increase in the duration but not the amplitude of EPSCs. The amplitude of EPSCs in the double mutant was 143.8 $\pm$ 45.9 pA, which was similar to that in the *unc-64* mutant. However, the duration of EPSCs increased from 22.3 $\pm$ 3.8 ms in *unc-64* to 81.0 $\pm$ 6.4 ms in *unc-64;slo-1* double mutants. Clearly, the removal of the SLO-1 current system in *unc-64* resulted in a significant increase of neurotransmitter release. Still, the release was only 20% of wild-type. This level of increase is consistent with the observed partial rescue of the movement and aldicarb-sensitive defects of the *unc-64* mutant by *slo-1* mutations.

Unexpectedly, the frequency of mEPSCs in the *unc-64; slo-1* double mutant was significantly higher than that in the *unc-64* mutant (Figure 7). One possible explanation for this is that a small fraction of SLO-1 channels might be active at resting conditions. A loss of SLO-1 function might influence the resting membrane potential and, thus, internal Ca^{2+} concentration. Alternatively, the absence of SLO-1 in the nerve terminal might influence the relationship between Ca^{2+} channels and release sites.

The amplitude of mEPSCs was essentially identical among wild-type, *slo-1* mutants, and *unc-64;slo-1* double mutants (details in the legends of Figures 5 and 7). However, the mean amplitude of mEPSCs in *unc-64* appeared somewhat larger. The source of the larger mEPSCs is unclear.

In summary, *slo-1* mutations prolonged synaptic release whether in an *unc-64* or wild-type genetic background. This prolongation in release resulted in an increase in EPSC quantal content, which was capable of alleviating the behavioral deficits of *unc-64* syntaxin mutant animals.

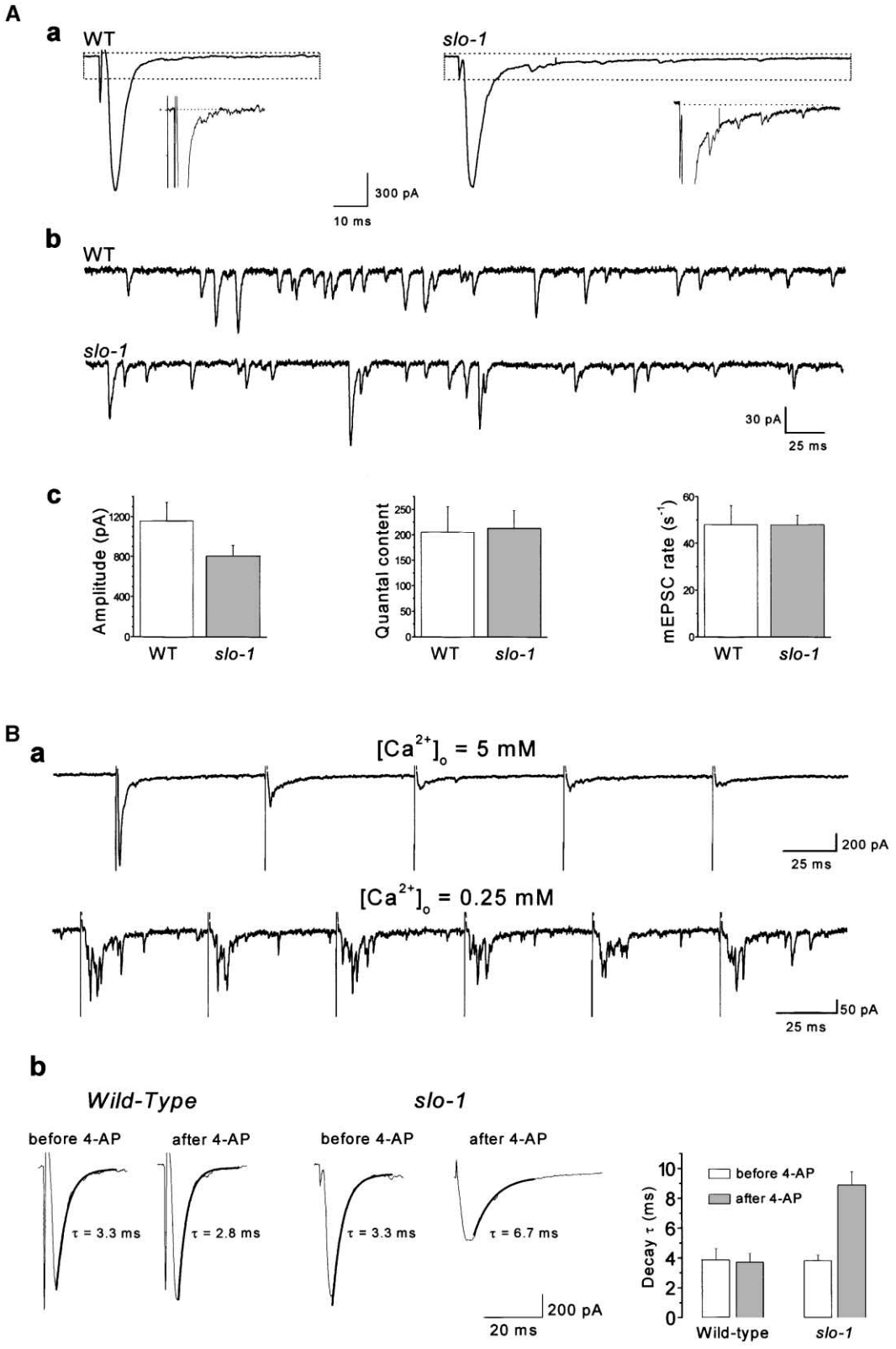

Figure 5. Properties of Evoked Neurotransmitter Release at the *C. elegans* NMJ

(A) *slo-1* mutant has no significant effect on EPSC quantal content at the neuromuscular junction at high $[Ca^{2+}]_o$ (5 mM).

(A_a) EPSCs from wild-type (WT) and *slo-1*(*md1745*) animals. Insets are the boxed regions of the main figures rescaled to show that EPSCs appear to take a longer time to decay to baseline in the *slo-1* mutant than in wild-type. However, this difference was not further quantified due to its small amplitude and variability in kinetic properties.

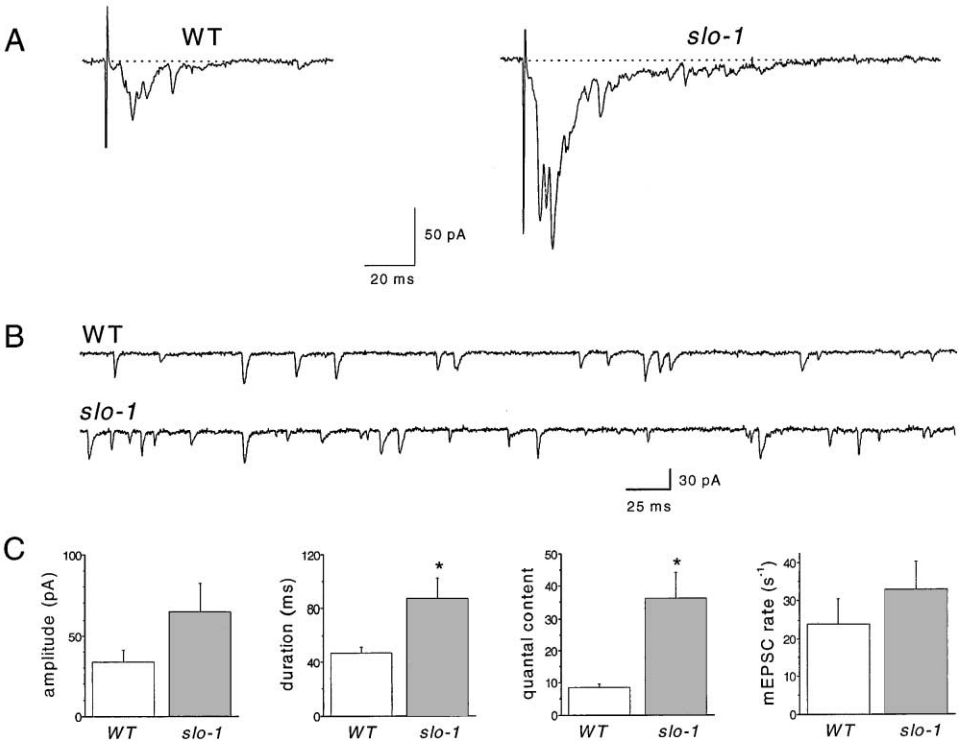

Figure 6. *slo-1* Mutation Prolongs the Duration and Increases the Quantal Content of Evoked Excitatory Postsynaptic Currents (EPSCs) at the Neuromuscular Junction at Lower $[Ca^{2+}]_o$ ($[Ca^{2+}]_o$ = 250 μM; $[Mg^{2+}]_o$ = 4 mM)

(A) EPSCs from wild-type (WT) and *slo-1*(*md1745*) animals showing longer duration and larger amplitude in the mutant.

(B) Representative traces of spontaneous miniature postsynaptic currents (mEPSCs) from WT and *slo-1*(*md1745*) animals.

(C) Quantification of EPSCs and mEPSCs in wild-type and *slo-1*(*md1745*) animals. Results are shown as mean ± SE. Asterisks (*) indicate statistically significant differences. No difference was present in average mEPSC amplitude (WT = 25.3 ± 2.9 pA; *slo-1* = 25.9 ± 2.9 pA) and current over time integral (WT = 62.8 ± 9.9 pA × ms; *slo-1* = 47.8 ± 10.2 pA × ms) between WT and *slo-1*. For EPSCs, n = 6 in WT, and n = 5 in *slo-1*. For mEPSCs, n = 10 in WT, and n = 8 in *slo-1*.

Several consecutive EPSCs from each prep were averaged to determine peak amplitude, duration (interval between the stimulation artifact and 90% decay of the peak amplitude), and quantal content (including only the area before the peak reached 90% decay). Individual EPSC traces are shown.

Discussion

In our screen, any of the more than 70 genes encoding K^+ channels in *C. elegans* (Salkoff, et al., 1999; Wei et al., 1996) might have appeared as effective modulators of neurotransmitter release. However, among the ten suppressor mutations analyzed, six were independent loss-of-function alleles of *slo-1* and none were mutations of other K^+ channels. It thus appears that this screen was able to discriminate between the different K^+ channel types, with regard to their importance in controlling neurotransmitter release. However, we recognize that other factors may be at work in our genetic screen. Not all K^+ channel loci may have equal mutagenicity, and homozygous mutations of some K^+ channel genes may be lethal. In addition, SLO-1 channels may be

(A_b) Representative traces of spontaneous miniature excitatory postsynaptic currents (mEPSCs) from wild-type and *slo-1*(*md1745*) animals.

(A_c) Quantification of EPSCs and mEPSCs in wild-type and *slo-1*(*md1745*). Results are shown as mean ± SE. There was no significant difference in EPSC amplitude and quantal content and in mEPSC frequency between the two groups. The amplitude (wild-type [WT] = 27.9 ± 2.7 pA; *slo-1* = 25.1 ± 0.8 pA) and current over time integral (WT = 52.4 ± 6.1 pA × ms; *slo-1* = 52.5 ± 4.3 pA × ms) of mEPSCs were also similar between the two groups. For EPSCs, n = 8 in WT, and n = 5 in *slo-1*. For mEPSCs, n = 10 in both WT and *slo-1*.

(B) The readily releasable pool of synaptic vesicles appears to be nearly depleted in response to a single stimulus in higher (5 mM) but not lower (250 μM) $[Ca^{2+}]_o$.

(B_a) Synaptic depression in response to repetitive stimulation in 5 mM but not 250 μM external $[Ca^{2+}]$. The stimulation rate was 7 Hz at 5 mM $[Ca^{2+}]_o$ and 10 Hz at 250 μM $[Ca^{2+}]_o$. At 5 mM $[Ca^{2+}]_o$, a large initial EPSC was followed by those with drastically reduced amplitudes. At 250 μM $[Ca^{2+}]_o$, however, the EPSC amplitude remained constant. Vertical straight lines are stimulation artifacts.

(B_b) Effects of 4-aminopyridine (4-AP) on EPSCs in wild-type and *slo-1*(*md1745*). A decay time constant (τ) was obtained by fitting the initial 20 ms decaying phase of EPSCs with a single exponential (shown in a thick black line). In the wild-type, neither the EPSC peak amplitude (control 1174 ± 350 pA, 4-AP 1104 ± 316 pA) nor the τ value (control 3.8 ± 0.8 ms, 4-AP 3.6 ± 0.7 ms) was changed following 4-AP application (n = 4). In the *slo-1* mutant, however, 4-AP significantly increased the τ value (control 3.8 ± 0.4 ms, 4-AP 8.9 ± 0.9 ms) (n = 3). The EPSC quantal content did not change significantly because the increase in the decay time constant was accompanied by a drop in EPSC peak amplitude (control 787 ± 171 pA, 4-AP 488 ± 103 pA).

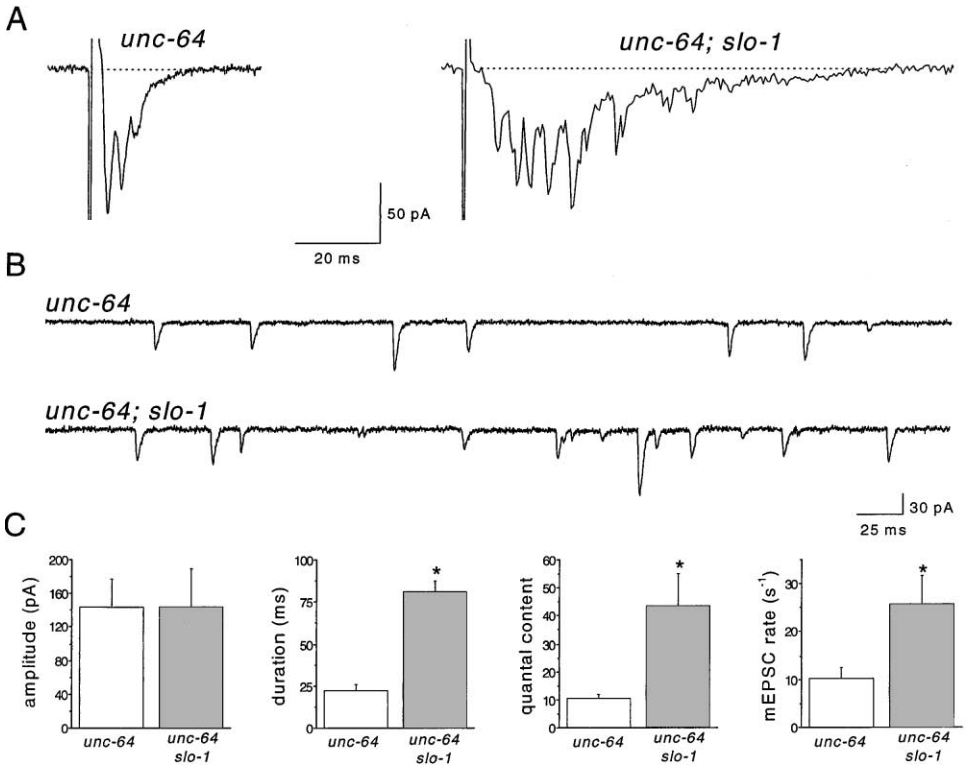

Figure 7. Reduced Quantal Content in *unc-64* Syntaxin Mutant and Enhancement by the *slo-1* Mutation at Higher $[Ca^{2+}]_o$ ($[Ca^{2+}]_o = 5$ mM; $[Mg^{2+}]_o = 5$ mM])

(A) Representative EPSCs from an *unc-64* mutant and an *unc-64;slo-1(js379)* double mutant. Addition of a *slo-1* mutation prolonged the EPSC duration and increased the quantal content significantly.

(B) Representative traces of spontaneous miniature postsynaptic currents (mEPSCs) from an *unc-64* mutant and an *unc-64;slo-1(md1745)* double mutant, showing higher frequency in the double mutant.

(C) Quantification of EPSCs and mEPSCs between *unc-64* and *unc-64;slo-1* mutants. Results are shown as mean ± SE. Asterisks (*) indicate statistically significant differences. The average mEPSC amplitude was 42.2 ± 5.3 pA in *unc-64*, and 26.8 ± 1.5 pA in *unc-64;slo-1* ($p < 0.05$). The average mEPSC current over time integral was 104.3 ± 15.5 pA × ms in *unc-64*, and 81.9 ± 9.9 pA × ms in *unc-64;slo-1*. The *slo-1* alleles used to construct double mutants were *md1745* and *js379*. For EPSCs, n = 5 in both *unc-64* and *unc-64;slo-1*. For mEPSCs, n = 13 in *unc-64*, and n = 8 in *unc-64;slo-1*.

EPSCs were also averaged to determine peak amplitude, duration, and quantal content as described in the legend of Figure 6. Individual EPSC traces are shown.

particularly abundant in synapses that are more directly responsible for the *unc-64* lethargic phenotype. Nevertheless, SLO-1 is likely to have major, if not unique, importance among K^+ channels as a regulator of neurotransmitter release in *C. elegans* and possibly in other systems.

Although direct observation of the role of SLO-1 has never been measured in presynaptic terminals of motor neurons, the contribution of the channel has been studied in other cells. The dominant role of SLO-1 over other K^+ channels in repolarizing an action potential which has a large Ca^{2+} component is illustrated by both developmental (Salkoff, 1985) and genetic (Elkins et al., 1986) studies from *Drosophila* flight muscles. Both SLO-1 and the 4-AP-sensitive Shaker current are present in those cells. However, the Shaker current does not appear to have an influence on the rate of repolarization if the SLO-1 current is present. Thus, the time course of action potential repolarization is always equally rapid regardless of whether the Shaker current (or 4-AP) is present as long as the SLO-1 current is present (Salkoff, 1985). Conversely, the absence of the SLO-1 current always results in longer duration action potentials, even if the Shaker current is present (Elkins et al., 1986; Salkoff, 1985). This seeming dominance of SLO-1 over the Shaker current may be the result of coupling activation not only to voltage but Ca^{2+} as well. Although similar recordings have not been done in presynaptic neuron terminals, a similarly large calcium component exists there too that may trigger SLO-1 in advance of a purely voltage-dependent current. As a result, it is not out of the question that SLO-1 may play a dominant role over other K^+ channels in some cells. Although only *slo-1* mutants were isolated from our screen, other K^+ channels might also be involved in the control of neurotransmitter release. For example, mutations of the *Drosophila* Shaker type K^+ channel augment neurotransmitter release at the NMJ at low Ca^{2+} conditions (Jan et al., 1977). The Shaker channel is 4-AP-sensitive. Our result shown in Figure 5B is also consistent with a 4-AP-sensitive K^+ channel being involved in regulating release at the *C. elegans*'s NMJ.

slo-1 mutations augmented neurotransmitter release both in the presence and absence of the *unc-64* syntaxin

mutation. In the absence of the *unc-64* mutation, however, the augmenting effect of *slo-1* on evoked postsynaptic currents was more obvious at reduced (250 μM) than at high (5 mM) $[Ca^{2+}]_o$. At 5 mM $[Ca^{2+}]_o$, approximately 200 vesicles were released per EPSC, resulting in a postsynaptic current of about 1 nA in amplitude. It is possible that under those conditions, either the number of synaptic vesicles that could be readily released was maximized or that available postsynaptic acetylcholine receptors were saturated. Therefore, it would be difficult to detect an augmenting effect of *slo-1* mutations on neurotransmitter release. Our results with repetitive stimulation at high Ca^{2+}, which showed acute synaptic depression, seem to suggest that a large proportion of the readily releasable vesicle population was released in response to a single motorneuron stimulation. If this were indeed the case, it would explain why, under conditions of high extracellular Ca^{2+}, neither the mutational ablation of SLO-1 nor the blockade of K^+ currents by 4-AP could elicit a response having significantly larger quantal content. We do not know what physiological $[Ca^{2+}]_o$ is in *C. elegans*. It seems likely though, given the acute synaptic depression seen in Figure $5B_a$, that it is far less than 5 mM. The facts that *slo-1* mutants are aldicarb-hypersensitive and that they suppress the phenotypes of the *unc-64* mutant suggest that SLO-1 K^+ channels play an important role in neurotransmitter release under physiological conditions. The observation of *slo-1* mutations augmenting neurotransmitter release in the *unc-64* mutant at 5 mM $[Ca^{2+}]_o$ reinforces the notion that the effectiveness of *slo-1* mutations on neurotransmitter release was not directly related to $[Ca^{2+}]_o$, but rather to the level of saturation of EPSC quantal content. Conceivably, in synapses of the central nervous system where Ca^{2+} sensors for vesicle fusion are far from saturation at normal release probability (Schneggenburger and Neher, 2000), BK channels could have a major role in regulating release.

Cytoplasmic Ca^{2+} concentrations required for triggering synaptic vesicle fusion vary from synapse to synapse. At the synaptic terminals of goldfish retinal bipolar neurons, exocytosis of synaptic vesicles requires relatively high cytoplasmic Ca^{2+} concentration with a threshold of 10 μM and half-maximal activation at 194 μM (Heidelberger et al., 1994). At the synaptic terminals of the rat calyx of Held, however, the Ca^{2+} sensitivity is higher, with a threshold of 1–2 μM $[Ca^{2+}]_i$. A brief increase of $[Ca^{2+}]_i$ from 10–25 μM is sufficient to reproduce the physiological release pattern (Schneggenburger and Neher, 2000; Bollmann et al., 2000). The threshold of $[Ca^{2+}]_i$ for synaptic release at the *C. elegans* NMJ is unknown. Regardless of its value, our results suggest that the threshold was achieved at the active zone during evoked responses even at 250 μM $[Ca^{2+}]_o$. Apparently, this is sufficient to activate SLO-1 to a significant level since we observed such an obvious prolongation of neurotransmitter release in *slo-1* mutants. This is in spite of the fact that SLO-1 heterologously expressed in *Xenopus* oocytes exhibited V_{50} values that were more positive than BK channels of humans (McCobb et al., 1995; Pallanck and Ganetzky, 1994; Tseng-Crank et al., 1994), mice (Butler et al., 1993), and *Drosophila* (Adelman et al., 1992). However, SLO-1 may have very different Ca^{2+} and voltage sensitivities in vivo. Association with β subunits (Knaus et al., 1994; Meera et al., 2000; Wallner et al., 1999; Weiger et al., 2000; Xia et al., 2000) or other proteins (Schopperle et al., 1998; Xia et al., 1998; Zhou et al., 1999), or phosphorylation by protein kinases (Esguerra et al., 1994; Robertson et al., 1993; Wang and Kotlikoff, 1996), or changes in channel sulfhydryl redox state (DiChiara and Reinhart, 1997; Wang et al., 1997) have all been reported to have profound effects on BK channel functional properties. The fact that BK channels have their activity modified by so many factors seems to indicate that the BK channel is a versatile channel system adapted to many purposes in a wide variety of cell types.

Previous studies have demonstrated that blockade of BK channels by iberiotoxin or charybdotoxin either augments (Robitaille et al., 1993; Robitaille and Charlton, 1992), reduces (Pattillo et al., 2001), or has no effect on neurotransmitter release (Fischer and Saria, 1999). These results suggest that BK channels may play a different role at different synapses. However, some of these discrepancies could also be due to a lack of adequate specificity of the toxins (Garcia et al., 1991) or to the presence of toxin-insensitive BK channels (Meera et al., 2000; Reinhart et al., 1989; Wang et al., 1992). In *Drosophila* Slo mutants, neurotransmitter release at NMJ appears to be reduced (Warbington et al., 1996). Our results are similar to those of Robitaille et al. (1993) who reported that application of iberiotoxin or charybdotoxin increases the amplitude of evoked excitatory postsynaptic potentials at the frog NMJ. Interestingly, the Ca^{2+} and Mg^{2+} concentrations used in their external solution (0.5 mM Ca^{2+}, 3.6 mM Mg^{2+}) are comparable to those at which we saw a large effect of *slo-1* mutations on neurotransmitter release (0.25 mM Ca^{2+}, 4 mM Mg^{2+}).

In the present study, we were able to avoid some of the uncertainties associated with the usage of channel blockers. The molecularly defined *slo-1* mutations remove BK channel function selectively and completely. Simultaneous measurements of both EPSCs and mEPSCs under voltage-clamp conditions allowed us to differentiate presynaptic effects of *slo-1* mutations from potential postsynaptic effects. Reintroduction of wild-type SLO-1 into *unc-64;slo-1* double mutants under the control of a neuron- or muscle-specific promoter further substantiated the presynaptic action of *slo-1* mutations. Our genetic and behavioral experiments bolster the conclusion that SLO-1 is an important regulator of synaptic release; *slo-1* mutants significantly suppressed the lethargy of *unc-64* animals and alleviated their resistance to aldicarb. In addition, EPG data also showed a role of SLO-1 in neurotransmitter release at inhibitory glutamatergic synapses in the pharynx, indicating that SLO-1 acts at excitatory, as well as inhibitory, synapses. All these results paint a picture consistent with the hypothesis that SLO-1 channels have a significant role in regulating neurotransmitter release.

Our results are consistent with a growing body of evidence suggesting that the influx of Ca^{2+} into presynaptic nerve terminals via voltage-sensitive Ca^{2+} channels not only triggers neurotransmitter release, but also activates colocalized BK channels which, in turn, terminate the release. At the presynaptic active zone, BK channels colocalize with Ca^{2+} channels (Issa and Hudspeth, 1994; Robitaille et al., 1993). BK channels appear

to be closer to Ca^{2+} channels than the Ca^{2+} sensor for synaptic release because EGTA inhibits release but not BK channels at the frog NMJ (Robitaille et al., 1993). During depolarization, cytoplasmic [Ca^{2+}] in the vicinity of Ca^{2+} channels can increase from about 100 nM at rest to 85–300 μM (Llinas et al., 1992; Tucker and Fettiplace, 1995; Yazejian et al., 2000). The activity of BK channels has been shown to be closely coupled to that of nearby voltage-gated Ca^{2+} channels (Marrion and Tavalin, 1998; Roberts et al., 1990; Yazejian et al., 2000). This close interaction is likely to be the mechanism by which SLO-1 K^+ channels regulate neurotransmitter release. These results, combined with the fact that the activity of BK channels is regulated both positively and negatively by a variety of factors, suggest that the function of presynaptic BK channels must be important for precise control of synaptic strength, which is fundamental to synaptic plasticity and other higher brain functions.

Experimental Procedures

Growth and Culture of *C. elegans*

C. elegans were grown at 22.5°C or room temperature, except where noted, on solid medium as described by Sulston and Hodgkin (1988). All mapping and complementation assays were performed using standard genetic methods (Herman and Horvitz, 1980). Aldicarb (2-methyl-2-[methylthio]proprionaldehyde O-[methylcarbamoyl] oxime) (Chem Services, Inc., West Chester, PA) was prepared as a 100 mM stock solution in 70% ethanol and added to the agar growth medium after autoclaving.

slo-1 Cloning and Minigene Constructs

A full-length SLO-1 clone (SLO-1a) was previously obtained in this lab by screening a cDNA library of embryonic *C. elegans* (Stratagene) (Wei et al., 1996). An alternatively spliced transcript, SLO-1b, was identified by RT-PCR. cDNAs of both splice variants were cloned into the ClaI and BamHI sites of the pBScMXT vector (Wei et al., 1994). A consensus sequence for translational initiation (Kozak, 1987) was added before the initiation codon in order to enhance expression in *Xenopus* oocytes. A third splice variant (SLO-1c) was identified by sequencing an EST clone (*yk640g9*, courtesy of Yuji Kohara, National Institute of Genetics, Japan).

Three *slo-1* minigenes were constructed by ligating different promoter sequences to the SLO-1a cDNA sequence. One minigene contained the native *slo-1* promoter (5239 bp). Another minigene (pBK3.1), a derivative of pRM248 (Nonet et al., 1998), contained the neuron-specific *snb-1* (synaptobrevin) promoter. A third minigene (pBK4.1) used pPD96.52 vector as the backbone, which contained the body-wall muscle-specific *myo-3* (myosin) promoter (Okkema et al., 1993). Schematic diagrams of the minigenes are shown in Figure 1C.

Genetic Analysis of *slo-1*

unc-64(e246) hermaphrodites (L4 stage) were mutagenized by exposure to 50 mM ethyl methanesulfonate for 4 hr. Second generation self-progeny (F2s) were screened for nonparalyzed animals. Six noncomplementing alleles of *slo-1(js100, js118, js379, js380, js381*, and *js382)* were isolated in a screen of 24,000 genomes. Each allele was backcrossed at least four times in order to remove extra nonassociated mutations, followed by outcrossing with N2 wild-type in order to determine the single mutant phenotype in an *unc-64*(+) background. *slo-1(js100)* was mapped by its ability to suppress *unc-64* paralysis (Sup). Using the Tc1 transposable element-containing strain, DP13 (Williams et al., 1992), this allele was mapped to the right arm of chromosome V. *e246/+; js100/+* males were crossed into DP13 hermaphrodites and random F1 progeny picked to individual plates. From the fraction of plates that segregated both Unc and Sup, Unc Sup double mutant progeny were selected and analyzed for presence of selected Tc1 polymorphic markers. This analysis placed *js100* to the right of stP105, within the same region containing a *C. elegans* ortholog of the mammalian and *Drosophila* BK channel (Adelman et al., 1992; Butler et al., 1993; McCobb et al., 1995; Pallanck and Ganetzky, 1994; Tseng-Crank et al., 1994). We named this gene *slo-1*.

The entire coding region of *slo-1* was sequenced in each allele to characterize the molecular lesions. Total RNA was prepared from mixed-stage animals. First-strand cDNA was synthesized using SUPERSCRIPT II RNase H^- Reverse Transcriptase (Gibco-BRL, Rockville, MD). Both oligo $(dT)_{12\text{-}18}$ and random hexamers were used as primers. First-strand cDNA then served as a template for PCR that used primers designed according to known *slo-1* cDNA sequences. The PCR products were sequenced without subcloning.

Transformation of *C. elegans*

Germline transformation was accomplished by coinjecting the plasmid of interest (10–20 ng/μl) with pBluescript carrier DNA (200 ng/μl) and a genetic marker. The genetic marker used was either the dominant $_p$*rol-6*::GFP marker (pPHGFP1 at 15–30 μg/ml) or the recessive *lin-15* marker (pJM23 at 50 μg/ml). When the *lin-15* marker was used, animals used for transformation had been crossed to contain the *lin-15(n765)* mutation (Mello et al., 1991; Huang et al., 1994). pBK3.1 and pBK4.1 were independently introduced into *unc-64; slo-1(js118)* double mutant animals using $_p$*rol-6*::GFP as the transformation marker, whereas the *slo-1* promoter-driven minigene was coinjected with the *lin-15* marker. To confirm that observed phenotypic changes following the injections were due to rescuing of *slo-1* mutations rather than overexpression of SLO-1, wild-type animals were also transformed with the minigenes to serve as controls.

SLO-1 Protein Localization

The native pattern of expression and localization of SLO-1 was evaluated by staining with a polyclonal antiserum raised against a portion of the Ca^{2+} bowl of the mouse BK channel (Knaus et al., 1995). Immunocytochemistry was performed as previously described using Bouin's fixative (Nonet et al., 1993). A *slo-1* promoter-driven SLO-1::GFP translational fusion was created by inserting GFP coding sequence into the SLO-1a cDNA at a location corresponding to a poorly conserved region of the protein between S8 and S9 (by replacing L706 and R707 of SLO-1 with GFP) (Figure 1C).

Behavioral and Pharmacological Assays

L4-staged animals were placed on fresh agar plates containing a thin *E. coli* lawn and grown at 22.5°C for 12–18 hr. Locomotion assays were performed at room temperature (20°C–22°C) by collecting serial CCD camera images at 5 s intervals with an LG3 frame grabber (Scion Corp., Frederick, MD). Plates were undisturbed on the microscope for 5–10 min before imaging initiated. Images of locomotion were collected prior to and after dropping a metal bar from a constant height onto the plate to mechanically excite the animals. Locomotion velocities were calculated between successive images by measuring the displacement in the position of the tail of each animal. Velocities from three pairs of images were calculated and averaged to assess both basal and stimulated locomotion.

Mutants were assayed for acute exposure to aldicarb. Sensitivity to aldicarb was examined by transferring 20–25 animals to plates containing aldicarb and assaying the time course of paralysis. Animals were considered paralyzed if they appeared hypercontracted and failed to move even if prodded with a platinum wire.

Electropharyngeograms

Electropharyngeograms (EPGs) were recorded from young adult hermaphrodites using an AC preamplifier (designed by David Brumley, University of Oregon) and LabView Acquisition software as previously described (Avery et al., 1995). Bath solution consisted of M9 with 2.5 mM serotonin added to stimulate pharyngeal pumping. Only recordings with at least ten pharyngeal pumps were analyzed.

Xenopus Oocyte Expression

Capped cRNAs were prepared with T3 RNA polymerase using a commercial kit (mMessage mMachine Kit, Ambion, Austin, TX) after linearization of the cDNA templates with NotI. The cRNAs were resuspended in nuclease-free water to a final concentration of 1 μg/μl. Approximately 50 nl cRNA was injected into each defolliculated

oocyte using a Drummond Nanojector (Drummond Scientific, Broomall, PA). Injected oocytes were incubated at 18°C in ND96 medium (96 mM NaCl, 2 mM KCl, 1.8 mM $CaCl_2$, 1 mM $MgCl_2$ and 5 mM HEPES [pH 7.5]) supplemented with sodium pyruvate (2.5 mM), penicillin (100 U/ml), and streptomycin (100 mg/ml).

Inside-out patches were obtained from the oocyte 2–7 days after cRNA injection using borosilicate glass pipettes that had a resistance of 1.5–3 mΩ (for macroscopic currents) or 5–8 mΩ (for single channel currents). [Ca^{2+}] was changed by exposing the cytoplasmic face of the patch to constant perfusion through a glass pipette. Current data was acquired at a sampling rate of 10 kHz or 50 kHz after filtering at 2 kHz. Leak current, determined by stepping from −60 to −80 mV, was automatically subtracted from the macroscopic current during acquisition. Delivery of voltage steps and acquisition of data was done with an Axopatch 200A amplifier and Clampex software (Version 7.0 or 8.0, Axon Instruments, Foster City, CA).

Composition of the pipette solution was 140 mM K^+ gluconate, 2 mM hemiMg^{2+} gluconate, and 5 mM HEPES (pH adjusted to 7.2 with KOH). Four internal solutions (pH 7.2) that differed in free [Ca^{2+}] were used to perfuse the cytoplasmic side of the patches. All internal solutions contained 140 mM K^+ gluconate and 10 mM HEPES. Besides, other components were added to adjust free [Ca^{2+}] (2 mM hemiCa^{2+} gluconate for 1 mM [Ca^{2+}], 0.2 mM hemiCa^{2+} gluconate for 100 μM [Ca^{2+}], 7.1 mM hemiCa^{2+} gluconate plus 5 mM HEDTA for 10 μM free [Ca^{2+}], and 8.3 mM hemiCa^{2+} gluconate plus 5 mM EGTA for 1 μM free [Ca^{2+}]). Free [Ca^{2+}] was calculated by EDTAETC (E . McCleskey).

Measurements of Synaptic Output at the Neuromuscular Junction

The NMJ preparation was modified from a previously described technique (Richmond et al., 1999; Richmond and Jorgensen, 1999). Briefly, adult worms were immobilized on sylgard-coated glass coverslips by applying a n-butyl-cyanoacrylate adhesive (Liquid Suture, B. Braun Medical Inc., Bethlehem, PA) along the dorsal side of the animals. A longitudinal incision was made in the dorsolateral region using a 30G needle (PrecisionGlide, Becton Dickinson, Franklin Lakes, NJ). After clearing the viscera, the cuticle flap was folded back and glued to the coverslip, exposing the ventral nerve cord and the two adjacent muscle quadrants. The prep was treated briefly (15 s) with collagenase (type A, Boehringer-Mannheim, Indianapolis, IN) at a concentration of 0.5 mg/ml. The prep was visualized with a Nikon Eclipse E600FN microscope equipped with a 40× water immersion lens and 10× eyepieces. Glass pipettes with a tip resistance of 3.5–7 MΩ were pulled from borosilicate glass, fire-polished, and used as electrodes for both nerve stimulation and current recordings. Classical whole-cell configuration was achieved by rupturing the patch membrane of a gigaohm seal formed between the recording electrode and a body-wall muscle cell. The cell was voltage-clamped at −60 mV to monitor mEPSCs and EPSCs. The EPSC was evoked by applying a 0.5 ms DC pulse (10–40 V) through the stimulation electrode placed in close apposition to the ventral nerve cord. Stimuli were generated by a S44 Stimulator, which was coupled to a SIU5 Stimulation Isolation Unit (Grass Instruments, Quincy, MA). Whole-cell currents were amplified with an Axopatch 200A amplifier and acquired with the Clampex software (Axon Instruments). Current data was sampled at a rate of 10 kHz after filtration at 2 kHz or 1 kHz.

The recording pipette was filled with a solution that contained: 120 mM KCl, 20 mM KOH, 4 mM $MgCl_2$, 5 mM Tris, 0.25 mM $CaCl_2$, 36 mM sucrose, 5 mM EGTA, and 4 mM Na_2ATP (pH adjusted to 7.2 with HCl). Two external solutions were used: high Ca^{2+} saline was composed of: 140 mM NaCl, 5 mM KCl, 5 mM $CaCl_2$, 5 mM $MgCl_2$, 11 mM dextrose, and 5 mM HEPES (pH adjusted to 7.2 with NaOH); low-Ca^{2+} saline differed from the high-Ca^{2+} saline only in concentrations of $CaCl_2$ and $MgCl_2$ (0.25 mM and 4mM, respectively). In experiments using 4-AP, the chemical was applied by perfusion after being dissolved in the high-Ca^{2+} external solution (pH readjusted to 7.2).

Data Analysis

Conductance-voltage relationships for macroscopic currents were plotted and fitted with a Boltzmann function. Conductance was then normalized to the maximal conductance of the Boltzmann fit.

About 60 s recordings of mEPSCs were analyzed in each NMJ preparation using MiniAnalysis (Synaptosoft, Inc., Decatur, GA) for measurements of frequency, amplitude, and area of mEPSCs. EPSCs were analyzed with Clampfit (Version 8.0, Axon Instruments) for amplitude and area. Several consecutive EPSCs were averaged to generate representative values of a particular preparation. Values of EPSC duration are based on the interval between the stimulation artifact and 90% decay of the peak amplitude of averaged peaks. The areas of both mEPSCs and EPSCs were integrals of the current trace over time (pA × ms).

Statistical analyses were done with SigmaStat (version 2.0, Jandel Corporation, San Rafael, CA). Either unpaired t test or ANOVA was used, depending on whether the number of groups being compared was more than two. $p < 0.05$ is considered statistically significant. All values are expressed as mean ± SE. "n" is equal to the number of animals.

Acknowledgments

The authors thank Janet Richmond for her kind help with setting up the technique for making the *C. elegans* NMJ prep in our labs. We also thank Kenneth Miller and James Rand for providing us with two *slo-1* alleles, Maria Garcia for the BK channel antibody, Pam Hoppe for $_p$*rol-6*::GFP, Yuji Kohara for an EST clone, and Andy Fire for pPD95.67 and pPD96.52 vectors. Gratitude also goes to Gonzalo Ferreira and members of the Salkoff and Nonet labs (in particular Aguan Wei, Maya T. Kunkel, Alex Yuan, and Nina Walton) for their intellectual contributions and/or technical assistance. We thank Jeanne M. Nerbonne for her critical comments about the manuscript. This work was supported by NIH grants to L.S. and M.L.N.

Received May 9, 2001; revised August 31, 2001.

References

Adelman, J.P., Shen, K.Z., Kavanaugh, M.P., Warren, R.A., Wu, Y.N., Lagrutta, A., Bond, C.T., and North, R.A. (1992). Calcium-activated potassium channels expressed from cloned complementary DNAs. Neuron *9*, 209–216.

Alfonso, A., Grundahl, K., Duerr, J.S., Han, H.P., and Rand, J.B. (1993). The Caenorhabditis elegans unc-17 gene: a putative vesicular acetylcholine transporter. Science *261*, 617–619.

Anderson, A.J., Harvey, A.L., Rowan, E.G., and Strong, P.N. (1988). Effects of charybdotoxin, a blocker of Ca^{2+}-activated K^+ channels, on motor nerve terminals. Br. J. Pharmacol. *95*, 1329–1335.

Avery, L. (1993). Motor neuron M3 controls pharyngeal muscle relaxation timing in Caenorhabditis elegans. J. Exp. Biol. *175*, 283–297.

Avery, L., Raizen, D., and Lockery, S. (1995). Electrophysiological methods. In Caenorhabditis elegans: Modern Biological Analysis of an Organism, H.F. Epstein and D.C. Shakes, eds. (San Diego: Academis Press), pp. 251–269.

Bollmann, J.H., Sakmann, B., and Borst, J.G. (2000). Calcium sensitivity of glutamate release in a calyx-type terminal. Science *289*, 953–957.

Butler, A., Tsunoda, S., McCobb, D.P., Wei, A., and Salkoff, L. (1993). mSlo, a complex mouse gene encoding "maxi" calcium-activated potassium channels. Science *261*, 221–224.

Chapman, P.F., Frenguelli, B.G., Smith, A., Chen, C.M., and Silva, A.J. (1995). The alpha-Ca^{2+}/calmodulin kinase II: a bidirectional modulator of presynaptic plasticity. Neuron *14*, 591–597.

Dent, J.A., Davis, M.W., and Avery, L. (1997). avr-15 encodes a chloride channel subunit that mediates inhibitory glutamatergic neurotransmission and ivermectin sensitivity in Caenorhabditis elegans. EMBO J. *16*, 5867–5879.

DiChiara, T.J., and Reinhart, P.H. (1997). Redox modulation of hslo Ca^{2+}-activated K^+ channels. J. Neurosci. *17*, 4942–4955.

Elkins, T., Ganetzky, B., and Wu, C.F. (1986). A Drosophila mutation that eliminates a calcium-dependent potassium current. Proc. Natl. Acad. Sci. USA *83*, 8415–8419.

Esguerra, M., Wang, J., Foster, C.D., Adelman, J.P., North, R.A., and

Levitan, I.B. (1994). Cloned Ca^{2+}-dependent K^+ channel modulated by a functionally associated protein kinase. Nature *369*, 563–565.

Farley, J., and Rudy, B. (1988). Multiple types of voltage-dependent Ca^{2+}-activated K^+ channels of large conductance in rat brain synaptosomal membranes. Biophys. J. *53*, 919–934.

Fischer, H.S., and Saria, A. (1999). Voltage-gated, margatoxin-sensitive potassium channels, but not calcium-gated, iberiotoxin-sensitive potassium channels modulate acetylcholine release in rat striatal slices. Neurosci. Lett. *263*, 208–210.

Garcia, M.L., Galvez, A., Garcia-Calvo, M., King, V.F., Vazquez, J., and Kaczorowski, G.J. (1991). Use of toxins to study potassium channels. J. Bioenerg. Biomembr. *23*, 615–646.

Gengyo-Ando, K., Kamiya, Y., Yamakawa, A., Kodaira, K., Nishiwaki, K., Miwa, J., Hori, I., and Hosono, R. (1993). The C. elegans unc-18 gene encodes a protein expressed in motor neurons. Neuron *11*, 703–711.

Heidelberger, R., Heinemann, C., Neher, E., and Matthews, G. (1994). Calcium dependence of the rate of exocytosis in a synaptic terminal. Nature *371*, 513–515.

Herman, R.K., and Horvitz, H.R. (1980). Genetic analysis of Caenorhabditis elegans. In Nematodes as Biological Models, Vol. 1: Behavioral and Developmental Models, B.M. Zuckerman, ed. (New York: Academic Press), pp. 227–262.

Huang, L.S., Tzou, P., and Sternberg, P.W. (1994). The lin-15 locus encodes two negative regulators of Caenorhabditis elegans vulval development. Mol. Biol. Cell *5*, 395–411.

Issa, N.P., and Hudspeth, A.J. (1994). Clustering of Ca^{2+} channels and Ca^{2+}-activated K^+ channels at fluorescently labeled presynaptic active zones of hair cells. Proc. Natl. Acad. Sci. USA *91*, 7578–7582.

Jan, Y.N., Jan, L.Y., and Dennis, M.J. (1977). Two mutations of synaptic transmission in Drosophila. Proc. R. Soc. Lond. B Biol. Sci. *198*, 87–108.

Katz, E., Ferro, P.A., Cherksey, B.D., Sugimori, M., Llinas, R., and Uchitel, O.D. (1995). Effects of Ca^{2+} channel blockers on transmitter release and presynaptic currents at the frog neuromuscular junction. J. Physiol. (Lond.) *486*, 695–706.

Knaus, H.G., Folander, K., Garcia-Calvo, M., Garcia, M.L., Kaczorowski, G.J., Smith, M., and Swanson, R. (1994). Primary sequence and immunological characterization of beta-subunit of high conductance Ca^{2+}-activated K^+ channel from smooth muscle. J. Biol. Chem. *269*, 17274–17278.

Knaus, H.G., Eberhart, A., Koch, R.O., Munujos, P., Schmalhofer, W.A., Warmke, J.W., Kaczorowski, G.J., and Garcia, M.L. (1995). Characterization of tissue-expressed alpha subunits of the high conductance Ca^{2+}-activated K^+ channel. J. Biol. Chem. *270*, 22434–22439.

Knaus, H.G., Schwarzer, C., Koch, R.O., Eberhart, A., Kaczorowski, G.J., Glossmann, H., Wunder, F., Pongs, O., Garcia, M.L., and Sperk, G. (1996). Distribution of high-conductance Ca(2+)-activated K+ channels in rat brain: targeting to axons and nerve terminals. J. Neurosci. *16*, 955–963.

Kohn, R.E., Duerr, J.S., McManus, J.R., Duke, A., Rakow, T.L., Maruyama, H., Moulder, G., Maruyama, I.N., Barstead, R.J., and Rand, J.B. (2000). Expression of multiple UNC-13 proteins in the Caenorhabditis elegans nervous system. Mol. Biol. Cell *11*, 3441–3452.

Kozak, M. (1987). At least six nucleotides preceding the AUG initiator codon enhance translation in mammalian cells. J. Mol. Biol. *196*, 947–950.

Lackner, M.R., Nurrish, S.J., and Kaplan, J.M. (1999). Facilitation of synaptic transmission by EGL-30 $G_q\alpha$ and EGL-8 PLCβ: DAG binding to UNC-13 is required to stimulate acetylcholine release. Neuron *24*, 335–346.

Lindgren, C.A., and Moore, J.W. (1989). Identification of ionic currents at presynaptic nerve endings of the lizard. J. Physiol. (Lond.) *414*, 201–222.

Llinas, R., Sugimori, M., and Silver, R.B. (1992). Microdomains of high calcium concentration in a presynaptic terminal. Science *256*, 677–679.

Marrion, N.V., and Tavalin, S.J. (1998). Selective activation of Ca^{2+}-activated K^+ channels by co-localized Ca^{2+} channels in hippocampal neurons. Nature *395*, 900–905.

Marshall, D.L., Vatanpour, H., Harvey, A.L., Boyot, P., Pinkasfeld, S., Doljansky, Y., Bouet, F., and Menez, A. (1994). Neuromuscular effects of some potassium channel blocking toxins from the venom of the scorpion Leiurus quinquestriatus hebreus. Toxicon *32*, 1433–1443.

Maruyama, I.N., and Brenner, S. (1991). A phorbol ester/diacylglycerol-binding protein encoded by the unc-13 gene of Caenorhabditis elegans. Proc. Natl. Acad. Sci. USA *88*, 5729–5733.

Maryon, E.B., Saari, B., and Anderson, P. (1998). Muscle-specific functions of ryanodine receptor channels in Caenorhabditis elegans. J. Cell Sci. *111*, 2885–2895.

Mathie, A., Wooltorton, J.R., and Watkins, C.S. (1998). Voltage-activated potassium channels in mammalian neurons and their block by novel pharmacological agents. Gen. Pharmacol. *30*, 13–24.

McCobb, D.P., Fowler, N.L., Featherstone, T., Lingle, C.J., Saito, M., Krause, J.E., and Salkoff, L. (1995). A human calcium-activated potassium channel gene expressed in vascular smooth muscle. Am. J. Physiol. *269*, H767–H777.

Meera, P., Wallner, M., and Toro, L. (2000). A neuronal beta subunit (KCNMB4) makes the large conductance, voltage- and Ca^{2+}-activated K^+ channel resistant to charybdotoxin and iberiotoxin. Proc. Natl. Acad. Sci. USA *97*, 5562–5567.

Meir, A., Ginsburg, S., Butkevich, A., Kachalsky, S.G., Kaiserman, I., Ahdut, R., Demirgoren, S., and Rahamimoff, R. (1999). Ion channels in presynaptic nerve terminals and control of transmitter release. Physiol. Rev. *79*, 1019–1088.

Mello, C.C., Kramer, J.M., Stinchcomb, D., and Ambros, V. (1991). Efficient gene transfer in C. elegans: extrachromosomal maintenance and integration of transforming sequences. EMBO J. *10*, 3959–3970.

Miller, K.G., Alfonso, A., Nguyen, M., Crowell, J.A., Johnson, C.D., and Rand, J.B. (1996). A genetic selection for Caenorhabditis elegans synaptic transmission mutants. Proc. Natl. Acad. Sci. USA *93*, 12593–12598.

Morita, K., and Barrett, E.F. (1990). Evidence for two calcium-dependent potassium conductances in lizard motor nerve terminals. J. Neurosci. *10*, 2614–2625.

Nonet, M.L., Grundahl, K., Meyer, B.J., and Rand, J.B. (1993). Synaptic function is impaired but not eliminated in C. elegans mutants lacking synaptotagmin. Cell *73*, 1291–1305.

Nonet, M.L., Saifee, O., Zhao, H., Rand, J.B., and Wei, L. (1998). Synaptic transmission deficits in Caenorhabditis elegans synaptobrevin mutants. J. Neurosci. *18*, 70–80.

Okkema, P.G., Harrison, S.W., Plunger, V., Aryana, A., and Fire, A. (1993). Sequence requirements for myosin gene expression and regulation in Caenorhabditis elegans. Genetics *135*, 385–404.

Pallanck, L., and Ganetzky, B. (1994). Cloning and characterization of human and mouse homologs of the *Drosophila* calcium-activated potassium channel gene, *slowpoke*. Hum. Mol. Genet. *3*, 1239–1243.

Pattillo, J.M., Yazejian, B., DiGregorio, D.A., Vergara, J.L., Grinnell, A.D., and Meriney, S.D. (2001). Contribution of presynaptic calcium-activated potassium currents to transmitter release regulation in cultured Xenopus nerve-muscle synapses. Neuroscience *102*, 229–240.

Raizen, D.M., and Avery, L. (1994). Electrical activity and behavior in the pharynx of Caenorhabditis elegans. Neuron *12*, 483–495.

Rand, J.B., and Russell, R.L. (1985). Molecular basis of drug-resistance mutations in C. elegans. Psychopharmacol. Bull. *21*, 623–630.

Rand, J.B., and Nonet, M.L. (1997). Synaptic transmission. In C. elegans II, D.L. Riddle, T. Blumenthal, B.J. Meyer, and J.R. Priess, eds. (Cold Spring Harbor, NY: Cold Spring Harbor Laboratory Press), pp. 611–644.

Reinhart, P.H., Chung, S., and Levitan, I.B. (1989). A family of calcium-dependent potassium channels from rat brain. Neuron *2*, 1031–1041.

Richmond, J.E., and Jorgensen, E.M. (1999). One GABA and two

acetylcholine receptors function at the *C. elegans* neuromuscular junction. Nat. Neurosci. *2*, 791–797.

Richmond, J.E., Davis, W.S., and Jorgensen, E.M. (1999). UNC-13 is required for synaptic vesicle fusion in *C. elegans*. Nat. Neurosci. *2*, 959–964.

Roberts, W.M., Jacobs, R.A., and Hudspeth, A.J. (1990). Colocalization of ion channels involved in frequency selectivity and synaptic transmission at presynaptic active zones of hair cells. J. Neurosci. *10*, 3664–3684.

Robertson, B.E., Schubert, R., Hescheler, J., and Nelson, M.T. (1993). cGMP-dependent protein kinase activates Ca-activated K channels in cerebral artery smooth muscle cells. Am. J. Physiol. *265*, C299–303.

Robitaille, R., and Charlton, M.P. (1992). Presynaptic calcium signals and transmitter release are modulated by calcium-activated potassium channels. J. Neurosci. *12*, 297–305.

Robitaille, R., Garcia, M.L., Kaczorowski, G.J., and Charlton, M.P. (1993). Functional colocalization of calcium and calcium-gated potassium channels in control of transmitter release. Neuron *11*, 645–655.

Saifee, O., Wei, L., and Nonet, M.L. (1998). The Caenorhabditis elegans unc-64 locus encodes a syntaxin that interacts genetically with synaptobrevin. Mol. Biol. Cell *9*, 1235–1252.

Salkoff, L. (1985). Development of ion channels in the flight muscles of *Drosophila*. J. Physiol. *80*, 275–282.

Salkoff, L., Kunkel, M.T., Wang, Z.W., Butler, A., Yuan, A., Nonet, M., and Wei, A. (1999). The impact of the Caenorhabditis elegans genome project on potassium channel biology. In Potassium Ion Channels, Molecular Structure, Function, and Diseases, Y. Kurachi, L.Y. Jan, and M. Lazdunski, eds. (San Diego: Academic Press), pp. 9–27.

Schneggenburger, R., and Neher, E. (2000). Intracellular calcium dependence of transmitter release rates at a fast central synapse. Nature *406*, 889–893.

Schopperle, W.M., Holmqvist, M.H., Zhou, Y., Wang, J., Wang, Z., Griffith, L.C., Keselman, I., Kusinitz, F., Dagan, D., and Levitan, I.B. (1998). Slob, a novel protein that interacts with the Slowpoke calcium-dependent potassium channel. Neuron *20*, 565–573.

Schreiber, M., and Salkoff, L. (1997). A novel calcium-sensing domain in the BK channel. Biophys. J. *73*, 1355–1363.

Sivaramakrishnan, S., Bittner, G.D., and Brodwick, M.S. (1991). Calcium-activated potassium conductance in presynaptic terminals at the crayfish neuromuscular junction. J. Gen. Physiol. *98*, 1161–1179.

Sulston, J., and Hodgkin, J. (1988). Methods. In The Nematode Caenorhabditis elegans, W.B. Wood and the Community of C. elegans Researchers, eds. (Cold Spring Harbor, NY: Cold Spring Harbor Laboratory Press), pp. 587–606.

Sun, X.P., Schlichter, L.C., and Stanley, E.F. (1999). Single-channel properties of BK-type calcium-activated potassium channels at a cholinergic presynaptic nerve terminal. J. Physiol. (Lond.) *518*, 639–651.

Tabti, N., Bourret, C., and Mallart, A. (1989). Three potassium currents in mouse motor nerve terminals. Pflugers Arch. *413*, 395–400.

Tseng-Crank, J., Foster, C.D., Krause, J.D., Mertz, R., Godinot, N., DiChiara, T.J., and Reinhart, P.H. (1994). Cloning, expression, and distribution of functionally distinct Ca^{2+}-activated K^+ channel isoforms from human brain. Neuron *13*, 1315–1330.

Tucker, T., and Fettiplace, R. (1995). Confocal imaging of calcium microdomains and calcium extrusion in turtle hair cells. Neuron *15*, 1323–1335.

Vatanpour, H., and Harvey, A.L. (1995). Modulation of acetylcholine release at mouse neuromuscular junctions by interaction of three homologous scorpion toxins with K^+ channels. Br. J. Pharmacol. *114*, 1502–1506.

Wallner, M., Meera, P., and Toro, L. (1999). Molecular basis of fast inactivation in voltage and Ca^{2+}-activated K^+ channels: a transmembrane beta-subunit homolog. Proc. Natl. Acad. Sci. USA *96*, 4137–4142.

Wang, G., Thorn, P., and Lemos, J.R. (1992). A novel large-conductance Ca^{2+}-activated potassium channel and current in nerve terminals of the rat neurohypophysis. J. Physiol. (Lond.) *457*, 47–74.

Wang, Z.W., and Kotlikoff, M.I. (1996). Activation of KCa channels in airway smooth muscle cells by endogenous protein kinase A. Am. J. Physiol. *271*, L100–L105.

Wang, Z.W., Nara, M., Wang, Y.X., and Kotlikoff, M.I. (1997). Redox regulation of large conductance Ca^{2+}-activated K^+ channels in smooth muscle cells. J. Gen. Physiol. *110*, 35–44.

Wangemann, P., and Takeuchi, S. (1993). Maxi-K^+ channel in single isolated cochlear efferent nerve terminals. Hear. Res. *66*, 123–129.

Warbington, L., Hillman, T., Adams, C., and Stern, M. (1996). Reduced transmitter release conferred by mutations in the slowpoke-encoded Ca^{2+}-activated K^+ channel gene of Drosophila. Invert. Neurosci. *2*, 51–60.

Waterston, R.H. (1988). Muscle. In The Nematode Caenorhabditis elegans, W.B. Wood and the Community of C. elegans Researchers, eds. (Cold Spring Harbor, NY: Cold Spring Harbor Laboratory Press), pp. 281–335.

Wei, A., Solaro, C., Lingle, C., and Salkoff, L. (1994). Calcium sensitivity of BK-type KCa channels determined by a separable domain. Neuron *13*, 671–681.

Wei, A., Jegla, T., and Salkoff, L. (1996). Eight potassium channel families revealed by the C. elegans genome project. Neuropharmacology *35*, 805–829.

Weiger, T.M., Holmqvist, M.H., Levitan, I.B., Clark, F.T., Sprague, S., Huang, W.J., Ge, P., Wang, C., Lawson, D., Jurman, M.E., et al. (2000). A novel nervous system beta subunit that downregulates human large conductance calcium-dependent potassium channels. J. Neurosci. *20*, 3563–3570.

Williams, B.D., Schrank, B., Huynh, C., Shownkeen, R., and Waterston, R.H. (1992). A genetic mapping system in Caenorhabditis elegans based on polymorphic sequence-tagged sites. Genetics *131*, 609–624.

Xia, X., Hirschberg, B., Smolik, S., Forte, M., and Adelman, J.P. (1998). dSLo interacting protein *1*, a novel protein that interacts with large-conductance calcium-activated potassium channels. J. Neurosci. *18*, 2360–2369.

Xia, X.M., Ding, J.P., Zeng, X.H., Duan, K.L., and Lingle, C.J. (2000). Rectification and rapid activation at low Ca^{2+} of Ca^{2+}-activated, voltage-dependent BK currents: consequences of rapid inactivation by a novel beta subunit. J. Neurosci. *20*, 4890–4903.

Yazejian, B., DiGregorio, D.A., Vergara, J.L., Poage, R.E., Meriney, S.D., and Grinnell, A.D. (1997). Direct measurements of presynaptic calcium and calcium-activated potassium currents regulating neurotransmitter release at cultured Xenopus nerve-muscle synapses. J. Neurosci. *17*, 2990–3001.

Yazejian, B., Sun, X.P., and Grinnell, A.D. (2000). Tracking presynaptic Ca^{2+} dynamics during neurotransmitter release with Ca^{2+}-activated K^+ channels. Nat. Neurosci. *3*, 566–571.

Zhong, Y., and Wu, C.F. (1991). Altered synaptic plasticity in Drosophila memory mutants with a defective cyclic AMP cascade. Science *251*, 198–201.

Zhou, Y., Schopperle, W.M., Murrey, H., Jaramillo, A., Dagan, D., Griffith, L.C., and Levitan, I.B. (1999). A dynamically regulated 14-3-3, Slob, and Slowpoke potassium channel complex in Drosophila presynaptic nerve terminals. Neuron *22*, 809–818.

Accession Numbers

The SLO-1a, SLO-1b, and SLO-1c cDNA sequences have been deposited at the GenBank with accession numbers of AF431891, AF431892, and AF431893, respectively.